JOURNAL OF GEOPHYSICAL RESEARCH, VOL. 101, NO. C5, PAGES 12,079–12,086, MAY 15, 1996

Intratidal variations in stratification and mixing in the Hudson estuary

H. M. Nepf
Civil and Environmental Engineering, Massachusetts Institute of Technology, Cambridge

W. R. Geyer
Woods Hole Oceanographic Institution, Woods Hole, Massachusetts

Abstract. This study represents a detailed examination of intratidal variations in boundary-layer structure in a relatively narrow, straight section of the Hudson river estuary during high river discharge. The presence of active mixing is inferred from estimates of the Richardson number. The maximum height above bed to which mixing occurs is comparable during flood and ebb; however, the regions of mixing differ in density structure. During the flood, active mixing is confined to a well-mixed near-bed layer, whereas during the ebb, active mixing occurs throughout regions of significant stratification. Tidal straining maintains stratification during the ebb, while it promotes the growth of a uniform bottom, mixed layer during the flood. In general, maximum and minimum near-bed stratification occur during late ebb and flood, respectively, reflecting the dominant role played by tidal straining in determining intratidal variation. Vertical stretching was also found to be an important term in the stratification balance during the ebb.

1. Introduction

Temporal variations in stratification in estuaries are controlled by the competing mechanisms of advection and mixing. For the mean flow field, that is, the estuarine circulation, *Linden and Simpson* [1986, 1988] experimentally documented the following feedback mechanism between the mean advection and turbulent mixing. The baroclinic circulation promotes stratification by carrying lighter river water over heavier ocean water, that is, the differential advection of salinity creates stratification. As the stratification increases, vertical mixing of momentum is inhibited, and the sheared circulation is reinforced. Alternatively, as turbulent mixing increases, the stratification is reduced directly by mixing and indirectly by a reduction in shear. Thus mixing diminishes the estuarine circulation, reducing its stratifying influence. The diminished stratification then promotes further mixing. Using energy considerations, *Nunes et al.* [1989] demonstrated how this positive feedback can promote large changes in local stratification with only moderate changes in tidal stirring energy. *Simpson et al.* [1990] extended this concept to intratidal variations by focusing on the differential advection associated with the tidal current boundary layer. Because the tidal shear changes sign during the tidal cycle, this process, called tidal straining, will promote stratification during the ebb, when the boundary layer shear augments the mean estuarine circulation but will diminish it during the flood, when the boundary layer shear opposes the mean.

Using detailed measurements of velocity and density, this paper examines intratidal variation in stratification and boundary layer structure in a partially stratified estuary. In particular, we focus on near-bed stratification and the processes which dictate its evolution. Processes of mean advection, tidal straining, vertical mixing, and vertical stretching associated with a bathymetrically forced convergence zone are found to be important.

Paper number 96JC00630.
0148-0227/96/96JC-00630$09.00

2. Observational Program

The field site (Figure 1) was located approximately 3000 m south of the George Washington Bridge in the Hudson river estuary. This reach is 10–20 m deep, roughly 1000 m wide, and unusually straight because of the Palisades, a resistant rock formation that runs along the west bank of the river. During the study, April 30 to May 3 of 1993, high river discharge, $\sim$2000 $m^3 s^{-1}$, provided a mean outflow velocity of 19 cm s^{-1} within the reach. Tidal velocities increased from 1.2 to 1.5 m s^{-1} over the study period, reflecting a neap to spring transition. The vertical velocity difference due to the estuarine circulation was $\sim$30 cm s^{-1}. The estuary was moderately stratified, and the maximum top to bottom salinity difference, occurring in the deepest section of the river, decreased from 18 to 12 practical salinity units (psu) as vertical mixing increased toward spring tide conditions. The longitudinal salinity gradient ranged between 0.4–1 psu km^{-1}.

Nineteen stations were selected to capture both lateral and longitudinal structure so that spatial as well as temporal variability could be examined. These stations are shown by circles on Figure 1b. On April 30 and May 2 the central transect, C1–C5, was traversed and sampled hourly for 12 hours. On May 1 an "I" configuration, comprised of the north and south transects, S1–S5 and N1–N5, and the longitudinal transect I1–I4, was similarly traversed hourly for 12 hours. On April 29 and May 3, longitudinal surveys were conducted to characterize estuarine conditions over a 25-km span from the southern end of Manhattan Island (the Battery) to north of the George Washington Bridge.

Velocity measurements were made using a ship-mounted, 1.2-MHz, narrow-banded, acoustic Doppler current profiler. The vertical resolution for the velocity was 1 m, beginning 3.5 m below the surface and extending to approximately 85% of

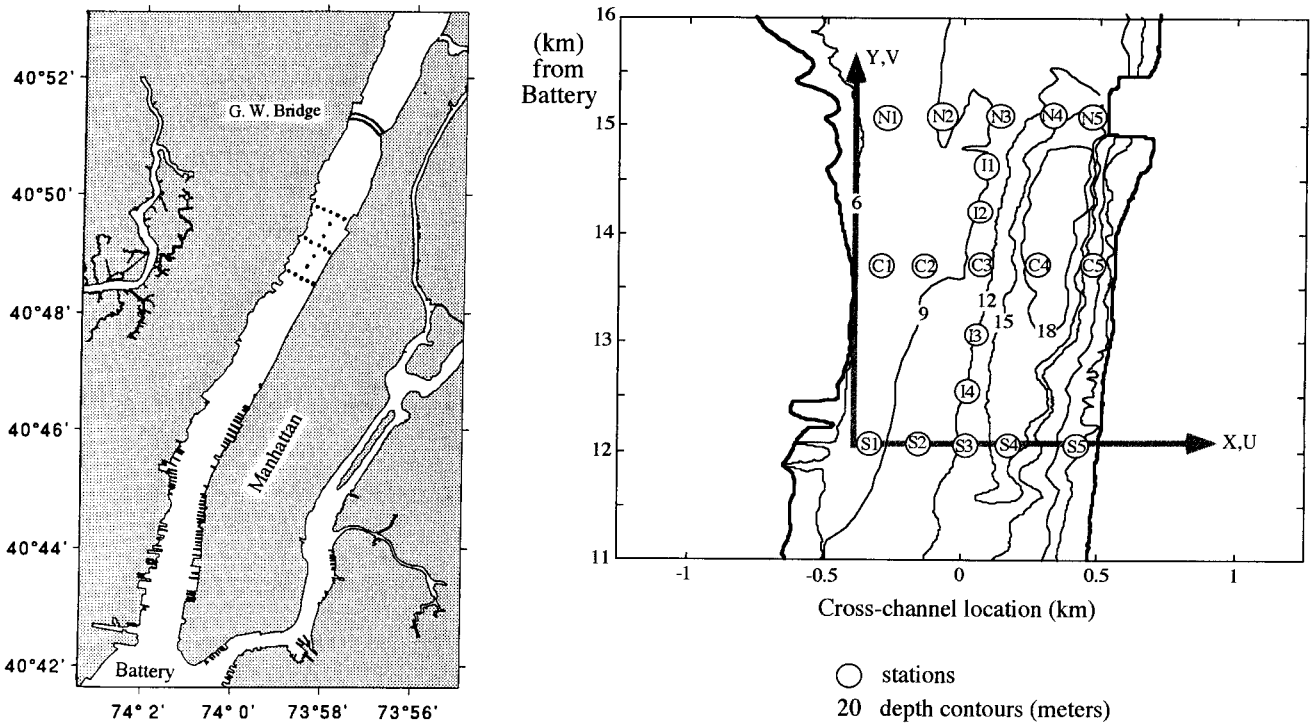

Figure 1. Hudson river estuary. The 19 measurement stations (marked by dots) are located 3000 m south of the George Washington Bridge.

the water depth. The velocity was rotated into river coordinates in which V is positive upstream and U is the cross-stream direction and is positive toward Manhattan. The vertical coordinate, z, is generally taken as zero at the bed and positive upward. In cases where several stations are plotted together in contour, z is taken as zero at the water surface to avoid distorting the relative depth positions at different stations.

Profiles of salinity were made using an Ocean Sensors Inc. OS200 conductivity-temperature-depth profiler. The vertical resolution for these profiles is 0.25 m, and the measurement error is approximately 0.04 psu. Coincident with the time of each cast a 1-min-averaged velocity profile was calculated from the raw velocity record. These profiles have a total mean error of approximately 10 cm s^{-1} based on bottom tracking (the largest source of error), noise, and turbulent fluctuation [*Geyer and Signell*, 1990].

In order to estimate boundary layer shears, the mean profiles were extrapolated to the bed. The extrapolation matched the profile slope at the end of the measured data, assumed zero velocity at the bed, and fit a parabolic profile in between. Typically, one or two points, that is, 1–2 m of profile, were added. A logarithmic profile fit was also examined. At peak flows the parabolic and logarithmic fits agreed to within 10%, with the logarithmic fit producing greater shears very near the bed (within 1 m). Near slack the logarithmic fit was faulty, because it could not accommodate near-bed flow reversals, for example, hour 18 in Figure 2. For simplicity the parabolic fit was used throughout the tidal cycle.

The Richardson number was calculated at 1-m resolution using both longitudinal (V) and cross-stream (U) velocity profiles and the coincident density profile.

$$Ri = -\frac{g}{\rho}\frac{\partial\rho/\partial z}{[(\partial U/\partial z)^2 + (\partial V/\partial z)^2]} = N^2/S^2, \qquad (1)$$

where ρ is density, g is the acceleration of gravity, U and V are the components of horizontal velocity, N is the buoyancy frequency, and S the total shear. Equation (1) was used to characterize the state of mixing within the water column, that is, for Ri less than a critical value, Ri_c, vertical mixing was expected to occur via shear instability. The value chosen for Ri_c is discussed later in the paper.

3. Observations

3.1. Temporal Variation in Near-Bed Stratification

Figures 2 and 3 depict the hourly variation in velocity and salinity observed on May 1 at station S4. The hour labels represent the nearest integer hour in universal time. During the ebb (hours 1300–1700 UT), salinity stratification developed in the lower half of the water column and was maintained down to the bed (Figure 3). In contrast, during flooding, near-bed stratification was progressively diminished and a uniform mixed layer grew steadily between hours 1800 and 2300 UT. A similar cycle was observed at each station, producing maximum

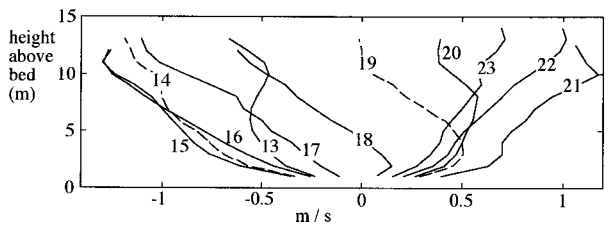

Figure 2. Profiles of velocity over one tidal cycle. Positive velocity is up-estuary. The profiles are marked by the nearest universal time hour. Dashed lines are used to distinguish between overlapping profiles.

and minimum near-bed stratification at the end of the ebb and flood, respectively. The depth scale vertical distribution of stratification also varied. At the end of the ebb, hour 1700 UT, the isopycnals are nearly horizontal and evenly spaced, indicating linear stratification over the entire depth. In contrast, at the end of the flood the water column was separated into a thick uniform layer capped by a strong halocline.

The shading in Figure 3 indicates regions of low Richardson number. As mentioned above, the Richardson number indicates the flow stability and the likelihood of active mixing. Two degrees of shading are shown to indicate regions in which Ri is less than 0.25 and 0.4. These values represent the following critical values of the Richardson number. First, on the basis of linear stability theory the theoretical threshold for mixing is $Ri_c = 0.25$ [*Miles*, 1961]. Observational evidence for its validity in geophysical flows has been documented by *Kunze et al.* [1990] and *Geyer and Smith* [1987]. However, the Richardson number estimates made for this study only reflect mean gradients and cannot account for the shear (and potential mixing) arising from internal wave activity which was present during the current study, as evidenced by echo sounder records. In addition, our Richardson number estimates cannot reflect instability and mixing on scales less than 1 m, the resolution of the velocity measurements. For both of these reasons a higher mixing threshold value was expected, that is, mixing is likely to occur at values of (1) greater than the theoretical prediction. To address these problems, a second critical value was defined on the basis of the observed vertical mixing of momentum and the values of Ri calculated from (1). During the flood the velocity maximum coincides with the top of the active boundary-generated mixing layer, that is, the momentum deficit boundary layer. The average Richardson number within this layer defines an observed threshold for mixing. To define this average value, points from individual velocity profiles were assigned to the active mixing layer if they fell below the velocity maximum. Because $\partial u/\partial z$ is small and Ri tends to a large value at the velocity maximum, this point was excluded from the average. Using data from all stations in the reach and all days of observation, $Ri_c = 0.4$. A similar analysis was not possible during the ebb because a momentum deficit boundary layer could not be clearly defined. So, for both flood and ebb we use $Ri < 0.4$ to indicate regions of potential mixing. In Figure 3 the active mixing region, defined by Ri_c, tracks the velocity maximum during the flood but consistently falls below it, suggesting that the contour $Ri_c = 0.4$ is a conservative estimate for the vertical extent of active mixing.

At station S4 (Figure 3), and similarly throughout the reach, the region of potential mixing extends to comparable heights during both flood and ebb. However, the flood and ebb conditions differ markedly in the strength of the stratification within the regions of low Ri. During the ebb the average stratification within the low-Ri region was -0.5 psu m^{-1}. This is an order of magnitude greater than that observed within the low-Ri region during the flood, -0.05 psu m^{-1}. These values reflect a flood-ebb asymmetry observed throughout the reach. During the flood the region of low Ri was coincident with the uniform layer near the bed. In addition, the two threshold values, $Ri = 0.25$ and 0.4, produced similar contours reflecting a sharp spatial transition between potential mixing and nonmixing regions. In contrast, during the ebb, no uniform layer was observed, and there was significant stratification in the low-Ri region.

The general variations in mixing and stratification discussed above and depicted in Figure 3 were representative of the

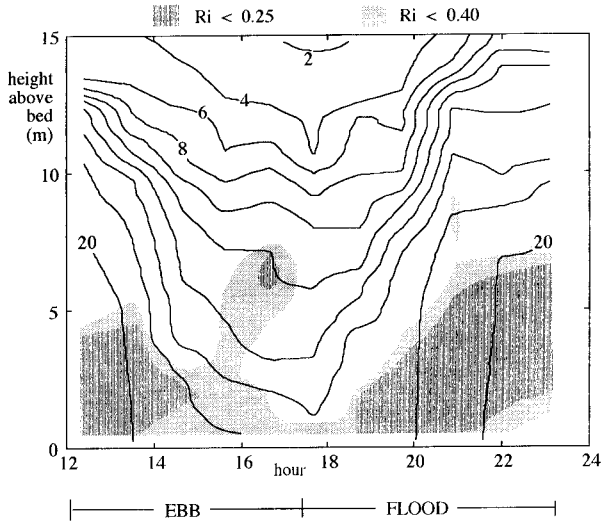

Figure 3. Depth-time contours of salinity constructed from individual hourly profiles measured simultaneously with the velocity profiles given in Figure 2. Richardson number estimates are indicated by shading.

structure throughout the reach on all days. However, as the flow increased from neap (April 30) toward spring (May 2) tide, the increasing tidal energy enhanced the vertical mixing. This was manifest in the tidal-maximum height of the potential mixing layer ($Ri = 0.4$ contour), which increased by an average of 2 m at all stations between April 30 and May 2.

3.2. Spatial Variation in Salinity Structure

Spatial variation in near-bed velocity and density structure was strongly influenced by depth variation. This is demonstrated by the cross section shown in Figure 4, selected for its large transverse variation in depth. The observations were taken on April 30 along the central transect (stations C1–C5 in Figure 1). The end of the flood and ebb are shown in Figures 4b and 4d to demonstrate the conditions of minimum and maximum near-bed stratification, respectively. The near-bed stratification is consistently larger at the shallower locations because of weaker mixing. In contrast, the tidal variation in near-bed stratification is larger in the deepest section because of greater tidal straining. To characterize these differences, we define a mean, near-bed stratification by $\Delta S/\Delta z$, where both differences are evaluated between the bed and 40% depth. Along the thalweg, the line of maximum depth, $\Delta S/\Delta z$ has a median value of -0.61 psu m^{-1} and varies between -0.02 and -1.20 psu m^{-1} (a 60-fold increase) between end-of-flood and end-of-ebb conditions. These values represent conditions in the thalweg on all 3 days. For the shallower locations at $X = 200$ and 400 m, $\Delta S/\Delta z$ has a median value of -1.42 psu m^{-1} and ranges between -1.00 and -1.84 psu m^{-1} (an approximately twofold increase). The lower median value in the thalweg reflects the greater average mixing within the deeper section. The variation in near-bed stratification reflects the effect of tidal straining. In the thalweg the velocity shear, and thus the tidal straining, is greater. This causes a greater decrease (increase) in stratification in the thalweg during the flood (ebb) relative to the shallower positions.

Figure 4 also indicates the mixing conditions, based on Ri, using the same shading as in Figure 3. The vertical extent of the low-Ri regions was significantly greater in the trench, such that

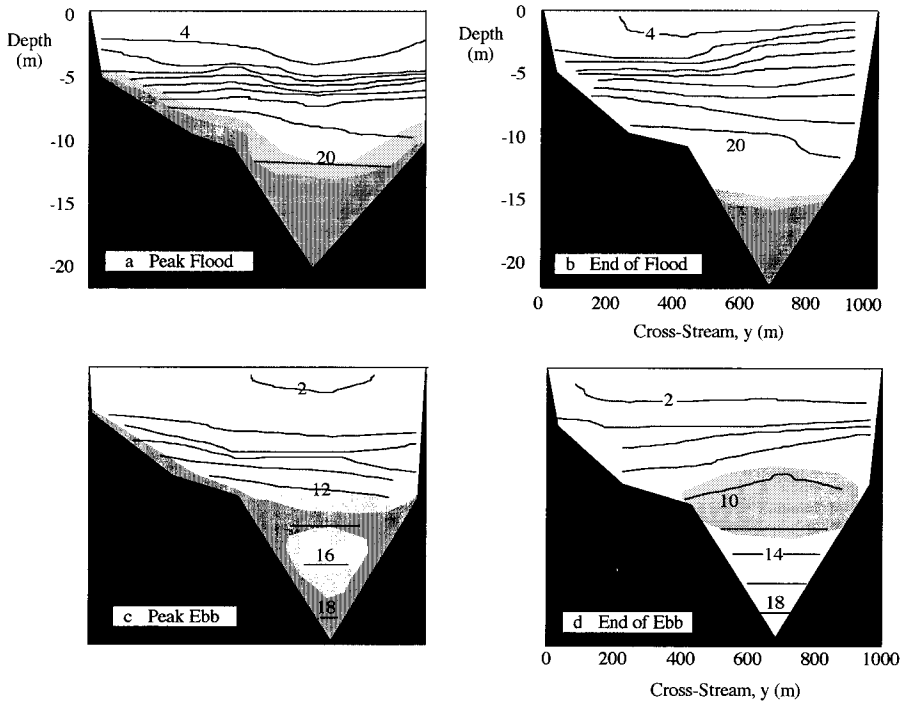

Figure 4. Central transect (C1–C5 in Figure 1). Note that depth is referenced to the surface in these plots to accommodate the variation in depth between the stations. Shading indicates regions of low Richardson number, as in Figure 3. (a) Salinity at peak flood; (b) salinity at end of flood; (c) salinity at peak ebb; (d) salinity at end of ebb.

the top of the potential mixing region was approximately level across the estuary. This lateral variation is most pronounced at peak flows and reflects the weaker stratification and greater velocities in the trench (see Figure 5). During the flood the low-Ri region and the near-bed uniform layer were coincident (Figure 4a). In contrast, during the ebb, low Richardson numbers occur within regions of stratification and were at times discontinuous with active-mixing regions elevated above the bed (see Figure 4c and Figure 3 at hour 1700 UT).

4. Discussion

4.1. Temporal Variation in Near-Bed Stratification

An equation describing the temporal evolution of stratification is readily derived by vertically differentiating the advection-diffusion equation for salt. The coordinate system used is that described in Figure 1b. Because the lateral gradients of salinity are several orders of magnitude weaker than the vertical and $u \ll v$, we assume $u(\partial S/\partial x) = 0$. In addition, we assume a horizontally uniform velocity and a constant along-channel salinity gradient. The resulting equation is

$$\frac{\partial}{\partial t}\frac{\partial S}{\partial z} = -\frac{\partial v}{\partial z}\frac{\partial S}{\partial y} - \frac{\partial}{\partial z}\left(w\frac{\partial S}{\partial z}\right) + \frac{\partial}{\partial z}\left(\frac{\partial}{\partial z}K_z\frac{\partial S}{\partial z}\right), \qquad (2)$$

where on the right-hand side the first term is strain, the second is stretch, and the third is diffusion.

Using observations collected on May 1 (predominantly stations S4, C4, and N4), each term in (2) was estimated, albeit with large uncertainty due to the poor resolution associated with the estimates of spatial gradients. The analysis was confined to the thalweg, where cross-channel flow was minimal because of bathymetric constraints, in order to minimize the contribution of cross-channel advection, which was poorly resolved by the measurement program and which we assume to be negligible in (2). The various terms were averaged over the bottom 40% of the depth to produce estimates for their contribution to the stratification in the lower layer. We focused on the central station (C4) for which longitudinal gradients were most easily defined. Figure 6 shows a time series of each term in (2). Because the vertical coordinate was positive upward, stable stratification was given by $\partial S/\partial z < 0$, so that $(\partial/\partial t)(\partial S/\partial z) < 0$ indicates increasing stratification. The specific analysis for each term is given below.

4.1.1. Temporal variation. The left-hand side of (2) represents the temporal variation in the salinity stratification for the near-bed region. The average near-bed stratification, $\partial S/\partial z$, was approximated as $\Delta S/\Delta z$, as described above. This quantity was estimated hourly at each station. Then the temporal variation in stratification was quantified using a central difference in time. This term is shown as a solid curve with circles in Figure 6.

4.1.2. Tidal straining. The first term on the right side of (2) represents the tidal straining due to vertical variation in the longitudinal velocity. The velocity shear, $\partial V/\partial z$ was estimated as $\Delta V/\Delta z$, where ΔV was simply the velocity at 40% depth, because $V = 0$ at the bed because of the no-slip condition. This linear approximation to the shear represents an average shear over the near-bed region. Because the actual velocity profiles tend toward a fuller shape (Figure 2), the linear approximation underestimates the shear near the bed and overestimates it toward the top of the layer. The along-channel salinity gradient, $\partial S/\partial y$, was obtained from measurements at the upstream and downstream ends of the section, separated by 3.2 km. The vertical shear and longitudinal salinity gradient

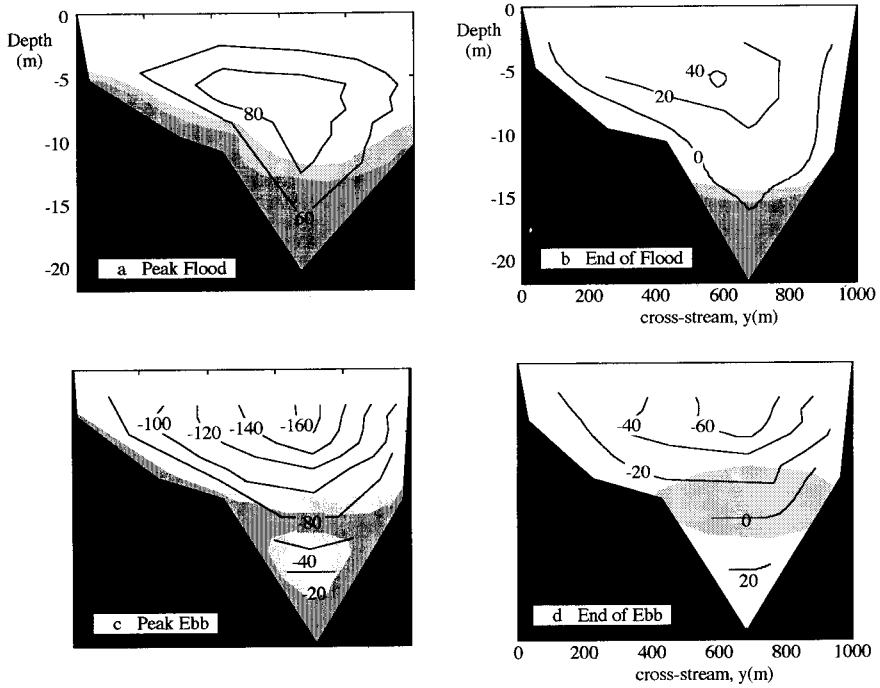

Figure 5. Central transect (C1–C5 in Figure 1). Note that depth is referenced to the surface in these plots to accommodate the variation in depth between the stations. Shading indicates regions of low Richardson number, as in Figure 3. (a) Velocity at peak flood; (b) velocity at end of flood; (c) velocity at peak ebb; (d) velocity at end of ebb.

both vary through the tidal cycle, as shown in Figure 7. Whereas the velocity shear varied smoothly, the longitudinal salinity gradient had a more irregular temporal variation, with the strongest gradient occurring close to the end of the ebb. This variation appeared to be associated with a near-bottom convergence in the thalweg, which intensified the horizontal gradient during the ebb. The convergence was evident in a comparison of ebb velocity profiles at different locations along the channel (Figure 8). Finally, the straining term was estimated as the product of the vertical shear and the longitudinal salinity gradient. Both the straining and the stretching term, described below, were averaged temporally to match the timescale of the central difference scheme used to estimate the temporal term.

As depicted in Figure 6, tidal straining enhanced stratifica-

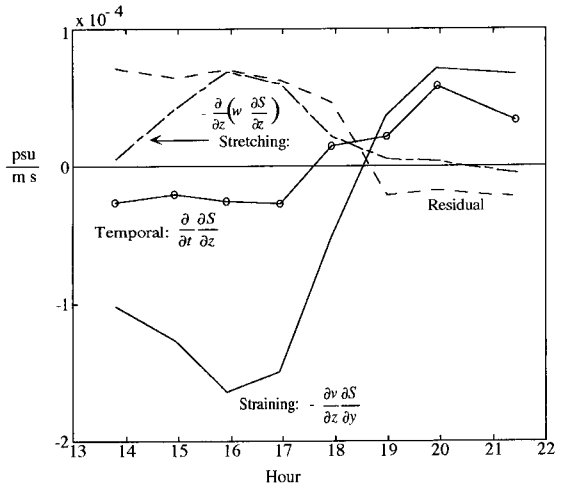

Figure 6. Time series of observed variation (curve with circles), straining (solid curve), and stretching (long and short dashed curve) of the near-bed stratification. The residual (dashed curve) represents both error and neglected terms such as vertical mixing. With z positive upward from the bed, $\partial S/\partial z < 0$ indicates stable stratification. The resulting sign convention for the estimated terms shown here is that negative variation corresponds to increasing stratification.

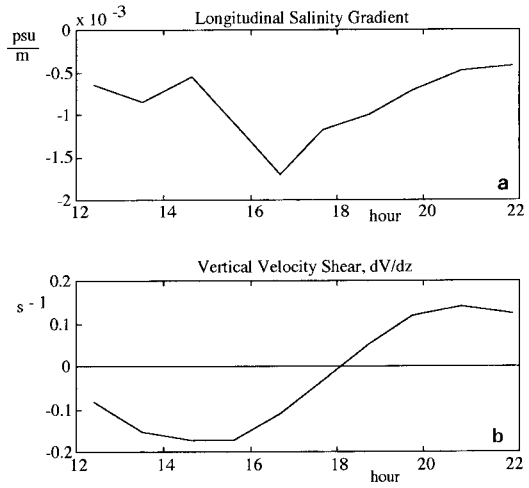

Figure 7. (a) Longitudinal salinity gradient within lower 40% of flow depth based on measurements at the upstream and downstream ends of the section. (b) Vertical shear across lower layer determined by the velocity at 40% depth and assuming $V = 0$ at the bed.

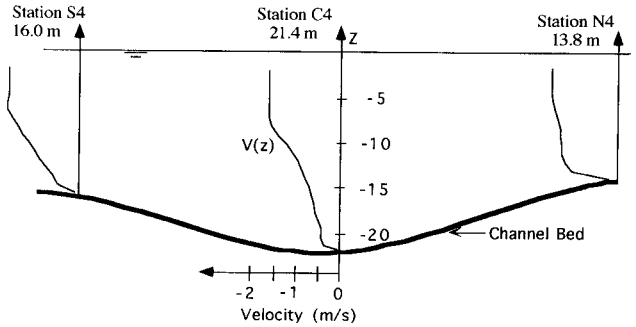

Figure 8. Ebb velocity profiles at three locations along the channel indicate a near-bottom convergence.

tion during the ebb (negative sign) and diminished it during the flood (positive sign). This cycle, however, was not completely reversible, as the magnitude of the ebb straining exceeded that of the flood. The tidally averaged straining was negative and represented the straining induced by the mean estuarine circulation. During the ebb and in the mean, tidal straining competed with vertical mixing to maintain stratification. During the flood, however, tidal straining reduced stratification and thus promoted vertical mixing. In addition, straining could actually produce mixing during the flood by straining the salinity field to a point of static instability, that is, by creating regions of $\partial S/\partial z > 0$. At the point of static instability the water column would mix rapidly, maintaining a lower layer of uniform salinity. This process of overstraining is discussed in a later section.

4.1.3. Vertical stretching. Profiles along the thalweg (Figure 8) indicate that during the ebb there was a strong variation in velocity near the bed between station N4 (located upstream at $y = 3200$ m) and the downstream stations C4 (at $y = 1800$ m) and S4 (at $y = 0$ m). On the basis of continuity this variation must be balanced by a divergence in either the cross-channel or vertical velocity. The geometry of the channel near the bed and between N4 and S4 does not permit a divergence in the lateral direction (Figure 1). Thus we assume that a vertical divergence balanced the along-estuary convergence and use this assumption to calculate the vertical velocity. The estimated vertical velocity reached a maximum value of 6 m h^{-1} during the latter portion of the ebb. Combined with the estimate of the local stratification at station C4, we estimated the second term on the right-hand side of (2), $(\partial/\partial z)(w\ \partial S/\partial z)$. This term, which we call vertical stretching, represents the stretching of the salinity field due to differential vertical advection. As the salinity field is stretched vertically, the stratification is diminished. As shown in Figure 6, this term was significant during the ebb and it acted to compensate in part for the tidal straining. Kinematically, the vertical velocity caused the flow to more closely parallel the sloping isohalines, decreasing the influence of straining.

It is important to emphasize that such a large convergence, as was observed here, could only occur over a limited spatial domain, since $\partial V/\partial y$ becomes smaller as the longitudinal scale increases. Thus the intense vertical velocity and vertical stretching of salinity gradients associated with the convergence can only be a local phenomenon which may vanish or change sign at other locations. The convergence at this site appears to be caused by an internal hydraulic response to the local bathymetry, specifically, the headland at the George Washington Bridge and a mild local constriction [*Geyer and Nepf*, 1996]. In addition, if the forcing for the convergence was the headland, its position relative to the measurement stations, that is, upstream, could explain why the convergence and vertical stretching were only observed during the ebb. We suggest that similar convergences may be present at other sites near significant bathymetric features and may similarly complicate the time variation of the salinity field.

4.1.4. Residual and vertical mixing. The last term in (2), vertical diffusion, was not measured directly but may be inferred from the residual of the other terms. The residual term shown in Figure 6 is calculated as the temporal variation minus the sum of the straining and stretching. In addition to vertical mixing, the residual also reflects the terms neglected in (2) and the errors in the three calculated terms. During the ebb the residual is positive. This is consistent with vertical mixing which acts to reduce stratification, positive by our sign convention. The negative residual during the flood results from the following. During the flood and once $\partial S/\partial z = 0$, overstraining produces buoyant instability ($\partial S/\partial z > 0$) and then mixing, which maintains $\partial S/\partial z = 0$. Under these conditions the straining term is positive (attempting to decrease stratification) and the temporal term is zero (because $\partial S/\partial z$ is maintained at zero) so that the residual is negative.

If during the ebb the residual is taken as the rate of change in stratification due to mixing, it can be used to approximate a mean, near-bed value of the vertical diffusivity, $\bar{K}_z$. Consider the near-bed region with a vertical extent, Δz, and an initial stratification $(\Delta S/\Delta z)|_i$. Under the action of a mean vertical diffusivity, $\bar{K}_z$, this region will be fully mixed, $(\Delta S/\Delta z) = 0$, on a timescale, $T_{\text{mix}} = \Delta z^2/4\bar{K}_z$. This leads to the following approximation.

$$\left.\frac{\partial}{\partial t}\frac{\partial S}{\partial z}\right|_{\text{mixing}} = \frac{(\Delta S/\Delta z)|_i}{T_{\text{mix}}} = \frac{\Delta S|_i \cdot 4\bar{K}_z}{\Delta z^3} = \text{residual}. \quad (3)$$

Hourly estimates of $\bar{K}_z$ were made from (3) using the residual term calculated from (2) and observed values of ΔS, defined above. For comparison, $\bar{K}_z$ was also estimated on the basis of a parabolic profile for turbulent diffusivity modified by a function of the Richardson number which represents the suppression of turbulence by stratification [*Dyer*, 1986; *Munk and Anderson*, 1948]. Specifically,

$$K_z(z) = \{\beta\kappa u_* z[1 - (z/h)]\}[1 + (10/3)Ri]^{-1.5}, \quad (4)$$

where $\beta \approx 1$ is a proportionality between the eddy viscosity and eddy diffusivity, $\kappa = 0.41$ is von Karman's constant, h is the flow depth, and u_* is the friction velocity approximated by a drag law, $u_* = \sqrt{C_d}V_{1\text{m}}$, with a drag coefficient $C_d = 0.001$. The near-bed average, $\bar{K}_z$, was simply taken as the numerical average over the near-bed region. Figure 9 shows that the estimate of $\bar{K}_z$ based on the residual in (2) agrees with the Munk-Anderson parameterization (3), suggesting that the residual term in (2) is a reasonable surrogate for vertical mixing during the ebb.

4.1.5. Overstraining. As mentioned above, during the flood, straining could produce mixing by creating regions of static instability, that is, $\partial S/\partial z > 0$. For clarity the conditions of straining that produce mixing will be called overstraining. Overstraining helps to create and maintain a mixed layer of increasing thickness, δ, observed during the flood (Figure 3). We estimated the contribution of overstraining to mixed layer growth by considering a uniform estuarine reach in which the

only contributors to stratification are straining and vertical mixing.

$$\frac{\partial}{\partial t}\frac{\partial S}{\partial z} = -\frac{\partial v}{\partial z}\frac{\partial S}{\partial y} - \frac{\partial}{\partial z}\left(\frac{\partial}{\partial z}K_z\frac{\partial S}{\partial z}\right) \quad (5)$$

Integrating (5) over the uniform layer, δ, we use the Leibnitz rule to simplify the left-hand term and note that there is no salt flux at the bed.

$$\frac{\partial}{\partial t}\int_0^{\delta}\frac{\partial S}{\partial z}\,dz - \left.\frac{\partial S}{\partial z}\right|_{z=\delta}\frac{\partial \delta}{\partial t} =$$

$$\int\frac{\partial v}{\partial z}\frac{\partial S}{\partial y}\,dz - \delta\left(\frac{\partial}{\partial z}K_z\frac{\partial S}{\partial z}\right)\Big|_{z=\delta} \quad (6)$$

The first term is zero by definition, that is, within the uniform layer, $\partial S/\partial z = 0$. Furthermore, we assume that vertical mixing vanishes for $z > \delta$, since Ri profiles suggest stable conditions just above the uniform layer. To maintain continuity of vertical salt flux, mixing must also vanish at $z = \delta$; thus the last term is zero. Finally, if we neglect the small vertical variations in $\partial S/\partial y$, the third term can be approximated by $V_{z=\delta}(\partial S/\partial y)$, and (6) can be rearranged to yield an expression for the mixed layer growth due to overstraining.

$$\frac{d\delta}{dt} = -\frac{V_{z=\delta}(\partial S/\partial y)}{(\partial S/\partial z)|_{z=\delta}}. \quad (7)$$

Using hourly observations during the flood, (7) was used to estimate the layer growth due to overstraining. At the deeper stations, for example, station S4, overstraining contributed 1 m h^{-1}. In contrast, at the shallower stations such as C3 the straining contributed only 0.4 m h^{-1}. This difference reflects the greater mean velocity and greater mean shears experienced at the thalweg stations. The observed uniform layer growth, attributable to both bed-generated mixing and overstraining, was 1.6 and 0.7 m h^{-1}, respectively. This suggests that overstraining contributed about 60% of the uniform layer growth at both shallow and deep locations.

4.2. Active Mixing and Well-Mixed Regions

During the flood (Figure 4a) the well-mixed region and the active-mixing region coincided and roughly occupied the area

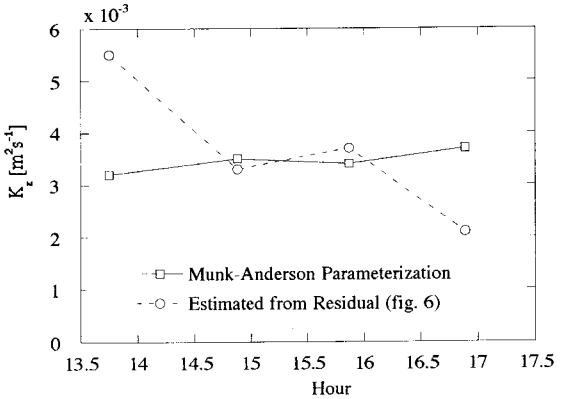

Figure 9. Ebb vertical diffusivity estimated from the residual term in Figure 6 and compared to diffusivity values estimated from the Munk-Anderson parameterization given in (4).

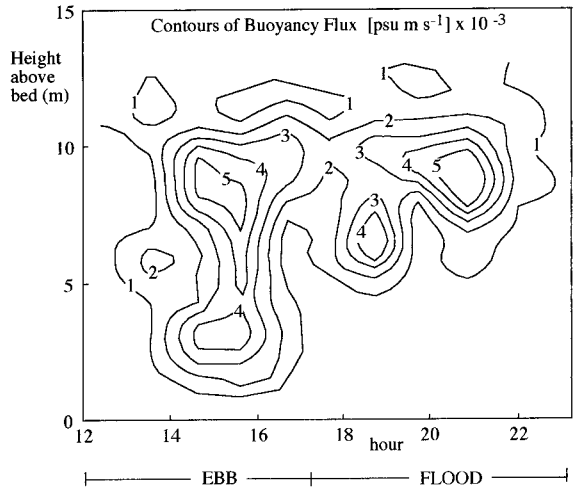

Figure 10. Contours of estimated of buoyancy flux, $\overline{w'S'}$, at station S4 based on a Munk-Anderson parameterization for $K_z(z)$.

below the velocity maximum. In this region, straining produced mixing as described by (7). However, above the velocity maximum the sign of the shear is reversed such that straining causes an increase in stratification which produces a sharp "lid" to the mixed layer. The suppression of mixing within the strongly stratified layer together with the baroclinic pressure gradient which accelerates the lower layer creates the sharp velocity maximum observed at the halocline during the flood.

The ebb spatial structure was different in that significant stratification was found in regions of low Richardson number. In addition, some regions of vigorous mixing ($Ri < 0.25$) were disconnected from the bed, suggesting that mixing was not purely boundary driven. Echo-sounding records revealed the characteristic "cats-eye" signature of Kelvin-Helmholtz billows, indicating some contribution to mixing by shear instability. Whether these instabilities were coupled to boundary layer processes or internal hydraulic phenomena was not determined.

Because the average stratification within the active mixing region was an order of magnitude greater during the ebb than the flood, greater near-bed buoyancy flux was expected during ebb. An estimate of the buoyancy flux,

$$\overline{w'S'} = -K_z(\partial S/\partial z) \quad (8)$$

was made using the Munk-Anderson parameterization for $K_z(z)$ given in (4) and the observed salinity gradients. The right side of (8) was estimated hourly throughout the tidal cycle at several stations. As an example, Figure 10 presents the contours of vertical flux plotted against depth and time for station S4. During the ebb, strong vertical flux was recorded over the entire water column. In contrast, during the flood, significant flux was only observed near the top of the boundary layer, $z > 6$ m. At most stations the depth-averaged buoyancy flux was 2–3 times greater during the ebb. The greater buoyancy flux during the ebb can be attributed to the tidal straining which maintains the stratification. Because the stratification is continually replenished, the mixing efficiency remains high; that is, mixing is effective in creating buoyancy flux. During the flood, stratification is not similarly maintained, so that once the salinity gradients are removed, mixing efficiency drops to zero,

because the fluid being mixed is already uniform so that no buoyancy flux results.

The above analysis is limited by the accuracy of (4) in representing the functional relation $K_z(Ri)$. To explore the sensitivity of the result, we examined a range of functional relations of the form

$$K_z = K_o(1 + Ri)^{-A}, \quad (9)$$

where K_o is the diffusivity within a neutral boundary layer, that is, the first bracket on the right side of (4). The exponent A was varied between 0 (for $K_z = K_o$) and 10. While the actual magnitude of flux varied between cases, the temporal and spatial distribution of vertical flux remained consistent, that is, greater flux was observed during the ebb for all but the highest exponent value. This result is not surprising considering the previously stated observation that the near-bed stratification was an order of magnitude greater during the ebb than the flood. Thus, unless the diffusivity was 10 times greater during the flood than ebb, for example, $A \geq 10$, the buoyancy flux will be greater for the ebb.

Finally, cross-channel variation in the boundary layer thickness was observed to correlate with flow depth, that is, during both flood and ebb the vertical extent of the low-*Ri* regions were significantly greater in the trench. This reflects the weaker stratification and greater velocities in the trench (see Figures 4 and 5). The latter produces greater advective and overstraining effects.

5. Conclusion

This study represents a detailed examination of intratidal variation in mixing and near-bed stratification. While the maximum vertical extent of mixing was comparable during flood and ebb, the regions of mixing were structurally different. During the flood, active mixing was confined to a well-mixed near-bed layer, whereas during the ebb active mixing occurred throughout regions of significant stratification. Because the stratification was maintained, a greater near-bed buoyancy flux was observed during the ebb. The maintenance of stratification during the ebb was attributed to tidal straining. During the ebb the effects of tidal straining were somewhat offset by vertical mixing and vertical stretching, both of which acted to diminish stratification. In contrast, during flood conditions, tidal straining promoted instability and mixing, that is, it did not compete with mixing to maintain stratification but rather complemented it to promote the growth of a uniform layer. In general, maximum and minimum near-bed stratification occurred during late ebb and flood, respectively, reflecting the dominant role played by tidal straining in determining intratidal variation.

Acknowledgments. This work was supported by the Hudson River Foundation. The authors would also like to thank Gail Kineke and Ole Madsen. During this work H. M. Nepf was supported as Postdoctoral Scholar at the Woods Hole Oceanographic Institution.

References

Dyer, K., *Coastal and Estuarine Sediment Dynamics*, 342 pp., John Wiley, New York, 1986.

Fischer, H., Mass transport mechanisms in partially stratified estuaries, *J. Fluid Mech.*, *53*, 671–687, 1972.

Geyer, W. R., and H. M. Nepf, Tidal pumping of salt in a moderately stratified estuary, in *Proceedings of the 7th International Biennial Conference on Physics of Estuaries and Coastal Seas*, Woods Hole, Mass., in press, 1996.

Geyer, W. R., and R. Signell, Measurements of tidal flow around a headland with a shipboard acoustic Doppler current profiler, *J. Geophys. Res.*, *95*, 3189–3197, 1990.

Geyer, W. R., and J. Smith, Shear instability in a highly stratified estuary, *J. Phys. Ocean.*, *17*, 1668–1679, 1987.

Jay, D., and J. Smith, Residual circulation in shallow estuaries, 1, Highly stratified, narrow estuaries, *J. Geophys. Res.*, *95*, 711–731, 1990.

Kunze, E., G. Briscoe, and A. J. Williams III, Interpreting shear and strain fine structure from a neutrally buoyant float, *J. Geophys. Res.*, *95*, 18,111–18,125, 1990.

Linden, P., and J. Simpson, Gravity-driven flows in a turbulent fluid, *J. Fluid Mech.*, *172*, 481–497, 1986.

Linden, P., and J. Simpson, Modulated mixing and frontogenesis in shallow seas and estuaries, *Cont. Shelf Res.*, *8*, 1107–1127, 1988.

Miles, J., On the stability of heterogeneous shear flows, *J. Fluid Mech.*, *10*, 496–508, 1961.

Munk, W., and E. Anderson, Notes on the theory of the thermocline, *J. of Mar. Res.*, *7*, 276–295, 1948.

Nunes, R., G. Lennon, and J. de Silva Samarasinghe, The negative role of turbulence in estuarine mass transport, *Estuarine, Coastal Shelf Sci.*, *28*, 361–377, 1989.

Simpson, J., J. Brown, J. Matthews, G. Allen, Tidal straining, density currents, and stirring in the control of estuarine stratification, *Estuaries*, *12*, 125–132, 1990.

Tennekes, H., and J. Lumley, *A First Course in Turbulence*, MIT Press, Cambridge, Mass., 1990.

Turner, J. S., *Buoyancy Effects in Fluids*, Cambridge Univ. Press, New York, 1973.

W. R. Geyer, Woods Hole Oceanographic Institution, Bigelow 106, Woods Hole, MA 02543. (e-mail: rocky@gusty.whoi.edu)

H. M. Nepf, Room 48-425, Civil and Environmental Engineering, Massachusetts Institute of Technology, Cambridge, MA 02139.(e-mail: hmnepf@mit.edu)

(Received July 5, 1995; revised January 11, 1996;
accepted February 7, 1996.)